Optimum Design Process of Coaxial Magnetic Gear Using 3D Performance Prediction Method Considering Axial Flux Leakage

Seung-Hun Lee, So-Yeon Im, Jun-Yeol Ryu, and Myung-Seop Lim, *Senior Member, IEEE*

***Abstract*—This article proposes a rapid and optimum design method that considers axial flux leakage for a coaxial magnetic gear (CMG). Conventional CMG optimum design methods perform two-dimensional (2D) finite element analysis (FEA) to evade the long computational time of three-dimensional (3D) FEA. However, conventional design methods do not consider axial flux leakage and are therefore less accurate than computationally exhaustive optimum design through 3D FEA. Therefore, as an alternative to reduce computational time, this article proposes a method that considers axial flux leakage for predicting the CMG performance combining correlation coefficients and 2D FEA instead of 3D FEA. The correlation coefficient is determined as the ratio of the square of the radial direction air gap flux in the equivalent magnetic circuit (EMC) that considers axial flux leakage to the square of the radial direction air gap flux in the EMC that does not consider axial flux leakage. The electromagnetic performance of the CMG predicted by the proposed method is used to develop a surrogate model for reducing computational time during the optimum design process. Based on the surrogate model, the optimum CMG design is analyzed to fabricate a prototype, and the proposed design process is validated through experiments.**

***Index Terms*—Axial flux leakage, coaxial magnetic gear (CMG), equivalent magnetic circuit (EMC), multi-objective optimization.**

I. Introduction

MACHINE size reduction is a contentious research topic in many industries. As the size of a machine is inversely proportional to its speed at constant power, high-speed machines have high power densities. Therefore, it is desirable for a machine to operate at high speeds and low torques.

Recently, Vernier permanent magnet (PM) machines, magnetically geared machines (MGM), and derived machines have been proposed and studied to achieve high torque density. A Vernier PM machine with a larger number of pole pairs in the rotor than the number of stator teeth has been proposed to improve torque density [1]. The Halbach array was applied to an MGM, a structure that combines an electric motor and a magnetic gear (MG), to analyze its electromagnetic characteristics and optimize the design [2]. Even machines with high torque density at high speeds and low torques are often required to operate at low speeds and high torques. In most cases, this is accomplished using gears. Most gears are mechanical; however, MG has recently been proposed as an alternative. This is because power transmission through mechanical gears due to physical contact causes problems such as energy loss, noise, and tooth wear. Additionally, a lubrication system is required to reduce friction and prevent damage to the gearbox, specifically under the gear tooth. MG has the advantage of low noise, no tooth wear, and good protection from overloads because they transmit power without physical contact [3].

MG can be divided into those that do not and do use the magnetic flux modulation effect. An MG that does not use the magnetic flux modulation effect can be implemented in a form similar to a simple mechanical gear but has poor torque density and a lower speed ratio than a mechanical gear. To overcome this problem, a magnetic gear topology considering the magnetic flux modulation effect has been proposed [4]. Many types of MG utilize the magnetic modulation effect, among which coaxial MGs (CMGs) are the most representative. Atallah et al. proposed a high-performance CMG and explained its operation principles [5]. Fig. 1 presents a general CMG configuration. A CMG comprises an inner rotor yoke, an outer rotor yoke, an inner rotor PM, an outer rotor PM, and a pole piece (PP). The inner rotor has fewer poles and rotates at a higher speed than the outer rotor. A CMG generates torque by coupling the magnetic flux generated on one rotor side, modulated by passing it through a PP, with the magnetic flux generated on the opposite rotor side. Fig. 2(a) shows that the magnetic flux generated by the inner-rotor PM is modulated like a magnetic flux generated by more poles. This gives the impression that the inner-rotor

Manuscript received 28 March 2023; revised 22 June 2023 and 11 September 2023; accepted 17 November 2023. Date of publication 23 November 2023; date of current version 21 March 2024. Paper 2023-EMC-0118.R2, presented at the 2022 IEEE Transportation Electrification Conference and Expo, Asia-Pacific, Haining, China, Oct. 28–31, and approved for publication in IEEE Transactions on Industry Applications by the Electric Machines Committee of the IEEE Industry Applications Society [DOI: 10.1109/ITECAsia-Pacific56316.2022.99419866]. This work was supported by Samsung Electronics. *(Corresponding author: Myung-Seop Lim.)*

Seung-Hun Lee and So-Yeon Im are with the Department of Automotive Engineering (Automotive-Computer Convergence), Hanyang University, Seoul 04763, South Korea (e-mail: seunghun6137@hanyang.ac.kr; soyeon96@hanyang.ac.kr).

Jun-Yeol Ryu is with the Korea Automotive Technology Institute (KATECH), Cheonan 31214, South Korea, and also with the Department of Automotive Engineering, Hanyang University, Seoul 04763, South Korea (e-mail: jyryu@katech.re.kr).

Myung-Seop Lim is with the Department of Automotive Engineering, Hanyang University, Seoul 04763, South Korea (e-mail: myungseop@hanyang.ac.kr).

Color versions of one or more figures in this article are available at https://doi.org/10.1109/TIA.2023.3335894.

Digital Object Identifier 10.1109/TIA.2023.3335894

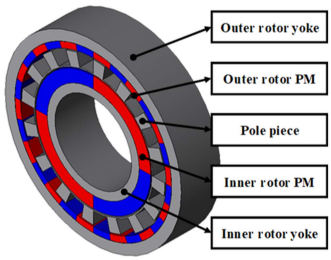

Fig. 1. Coaxial magnetic gear (CMG) configuration.

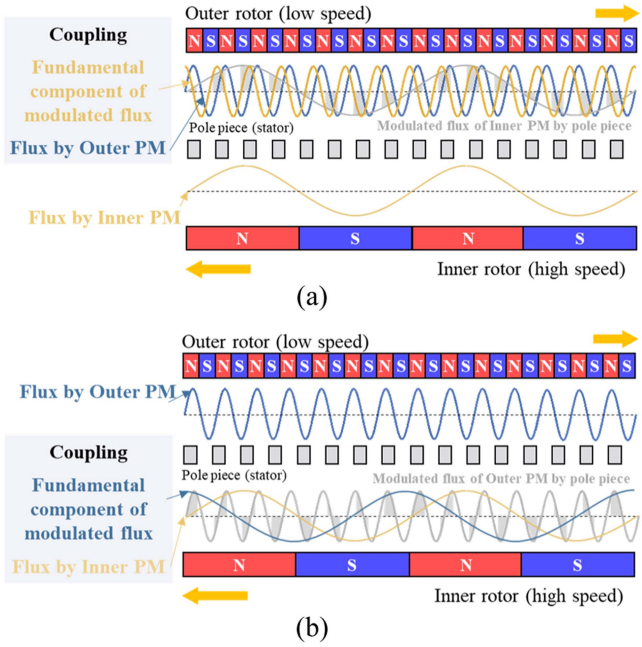

Fig. 2. Modulation effect. (a) Modulated magnetic flux by inner rotor permanent magnet (PM). (b) Modulated magnetic flux by outer rotor PM.

PM has the same number of poles as that generated by the outer-rotor PM. Similarly, Fig. 2(b) shows that the magnetic flux generated by the outer-rotor PM is modulated like a magnetic flux generated by a fewer number of poles. Thus, this gives the impression that the outer-rotor PM has the same number of poles as those generated by the inner-rotor PM. The flux modulation is determined by the number of poles in the inner- and outer-rotor PMs, and the number of PPs. To improve transmission torque, the number of PPs was selected as follows:

$$N_{\mathrm{PP}} = P_{\mathrm{in}} + P_{\mathrm{out}}, \tag{1}$$

where N_{PP}, P_{in}, and P_{out} are the number of PPs, pole pairs in the inner-rotor PM, and pole pairs in the outer-rotor PM, respectively. Furthermore, to synchronize the rotation speed of the outer rotor with the rotation speed of the inner rotor when the PP is stationary, the following equation can be used:

$$\omega_{\mathrm{in}} = -\frac{P_{\mathrm{out}}}{P_{\mathrm{in}}} \times \omega_{\mathrm{out}} = -G_r \times \omega_{\mathrm{out}}, \tag{2}$$

where ω_{in} is the inner rotor rotation speed, ω_{out} is the outer-rotor rotation speed, and G_r is the gear ratio.

Based on these principles, several studies have been conducted to improve the performance of CMGs. Jian et al. proposed a CMG with a Halbach array to achieve a torque density of excess 100 kNm/m^3 [6], [7]. Scheidler et al. noted that while magnetic gears typically have a lower torque density than mechanical gears, some types of magnetic gears appear to have the potential to achieve a torque density that is at least equivalent to certain mechanical gears when torque ratios are considered [8]. Jing et al. proposed a CMG with a Halbach array combined with a spoke structure and double-layer PM to increase the effective harmonics and reduce the torque ripple [9].

In addition, many methods have been proposed to analyze the performance of CMGs, and they can be classified based on three main perspectives. The first is an equivalent-network-based analysis method. Fukuoka et al. proposed an analysis method using reluctance network analysis [10]. Johnson et al. proposed a CMG analysis method that uses a linear two-dimensional (2D) equivalent magnetic circuit (EMC) [11]. Johnson et al. proposed a method for analyzing CMGs using a three-dimensional (3D) linear EMC [12]. The second perspective involves an analytical method based on a mathematical solution to the field equation. Lubin et al. calculated an analytical solution for the magnetic field distribution of a CMG using the Laplace and Poisson equations [13]. Shin and Chang calculated an analytical solution for the magnetic field distribution of a CMG using a 2D space harmonic analysis [14]. Zhao et al. calculated an analytical solution for magnetic field distribution by considering the magnetic saturation of a CMG using a harmonic modeling method [15]. The third perspective is a numerical-model-based analysis based on finite element analysis (FEA). FEA can be categorized as 2D FEA and 3D FEA. 2D FEA has the advantage of a shorter computational time than 3D FEA. However, compared with 2D FEA, 3D FEA provides results that are similar to that obtained in real experiments. Despite the high accuracy of 3D FEA, most CMGs have been analyzed using 2D FEA because of the longer computational time requirements of 3D FEA. Rasmussen et al. validated the performance of a CMG through 2D FEA and experiments, and found that as 2D FEA failed to consider the end effect, it caused errors [16]. Gerber and Wang compared the measurement results of CMG prototypes with those of 2D and 3D FEAs, suggesting various causes of error, and found that the representative reason was flux leakage [17]. Gerber and Wang found that the end effect can have a significant influence on the performance of MGs and MGMs, and proposed a method to estimate 3D FEA performance considering aspect ratio and 2D FEA performance [18]. However, the 2D FEA CMG performance can be overestimated compared with the 3D FEA CMG performance, although 3D FEA requires a significant computational time. Therefore, to predict the performance of an MG without using 3D FEA, a previous study, presented at the *2022 IEEE Transportation Electrification Conference and Expo, Asia-Pacific (ITEC Asia-Pacific)*, had proposed a method that considers both the axial flux leakage of 3D FEA and the relatively fast computational time of 2D FEA [19].

The remainder of this article is organized as follows. In Section II-B, the axial flux leakage permeance is described, and the proposed method is used to expand the CMG optimization

TABLE I
TARGET SPECIFICATIONS

Parameters	Value	Unit
Inner / Outer rotor pole pair	2 / 14	-
Inner / Outer rotor torque	2.4 / 16.8	Nm
Inner / outer rotor rotation speed	350 / 50	rpm
Outer rotor outer diameter	110	mm
Inner rotor inner diameter	48	mm
Inner / Outer air gap length	0.8	mm
PM residual flux density @90°C	1.19	T
PM relative recoil permeability	1.05	-
PM material	N42H	-

process based on the kriging surrogate model and sequential quadratic programming (SQP). Furthermore, the optimization results are used to fabricate prototypes, whose performance is experimentally validated. The target specifications for CMG optimization are listed in Table I. Section II describes the CMG performance prediction considering the axial flux leakage. Section III describes the optimal design process for a CMG using the method proposed in Section II. Section IV describes the experimental validation of the fabricated prototype CMG using the proposed CMG optimization design process. Finally, Section V concludes the article.

II. PROPOSED METHOD FOR 3D PERFORMANCE PREDICTION

Owing to electromagnetic losses, such as PM eddy current loss and iron loss, the torque ratio in the CMG is not equal to the reciprocal of the gear ratio. In addition, the CMG performance results obtained by 2D FEA may be overestimated because 2D FEA does not consider the end effect and 3D flux leakage. Fig. 3(a) shows that axial flux leakage paths exist in the PM and PP when analyzed using 3D FEA. Fig. 3(b) and (c) show the results of analyzing the magnetic flux density in the outer air gap using Fast Fourier Transform (FFT). From these results, the amplitude of all harmonic component, including the 14^{th} harmonic components, which is the main component that generates the outer rotor torque in both the radial and tangential magnetic flux densities, is reduced in 3D FEA compared to 2D FEA.

Fig. 4 shows the process of predicting the CMG performance of 3D FEA with 2D FEA by calculating the correlation coefficient through the EMC for the axial flux leakage, which is not considered in 2D FEA. The correlation coefficient is the square of the flux in the 3D EMC with considering the axial flux leakage divided by the square of the flux in the 2D EMC without considering the axial flux leakage. Although the magnetic flux calculation results calculated by FEA and EMC are different, the magnetic flux change ratio calculation results of FEA and EMC according to changes in design variables such as PM thickness, rotor yoke thickness, and PP angle are similar. According to the electromechanical energy conversion principle, the torque

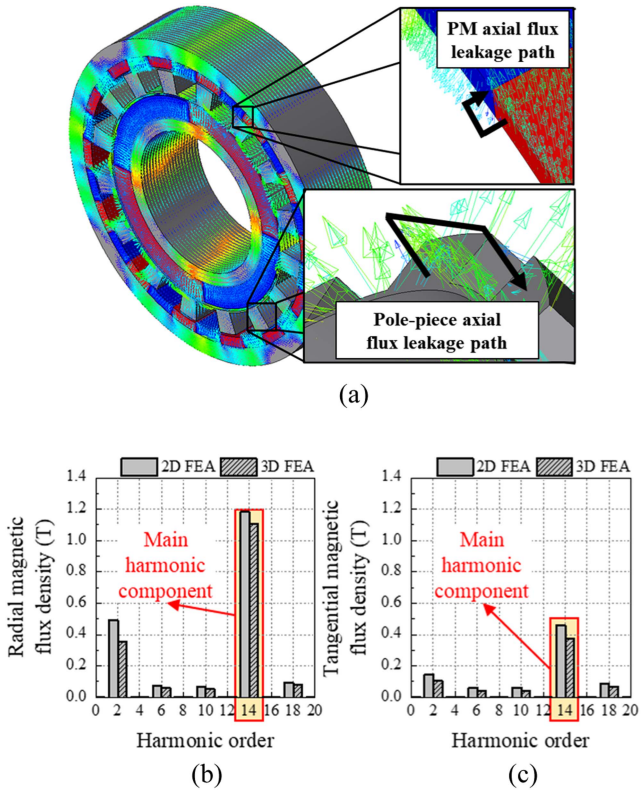

Fig. 3. Three-dimensional (3D) finite element analysis (FEA) results of CMG. (a) Axial flux leakage path at PM and pole piece (PP). (b) Fast Fourier Transform (FFT) results for radial magnetic flux density. (c) FFT results for tangential magnetic flux density.

is proportional to the square of the magnetic flux density in the air gap. Therefore, it can be assumed that the magnetic change ratio between 2D and 3D EMC obtained by the magnetic flux calculated in Steps 1 and 2 is the same as the torque change ratio between 2D and 3D FEA. Thus, this correlation coefficient was multiplied by the torque results from the 2D FEA to predict the torque from the 3D FEA. In addition, tangential elements were not considered in the 2D and 3D EMC. If tangential elements are modeled, more accurate results of magnetic flux can be obtained in EMC; however, because this article uses the magnetic flux change ratio between 2D and 3D EMC, only radial and axial elements are modeled without considering tangential elements to reduce the complexity of the EMC. Also, because nonlinearity, such as the saturation of iron, can be impactful in some designs, the magnetic flux can be calculated using a nonlinear EMC model. However, Johnson et al. showed that a linear model is still highly accurate for analyzing the torque performance of an idealized CMG design, indicating that the linear model is reasonable [20], [21]. In addition, linear EMC models are used because they guarantee a very fast computational time compared with nonlinear EMC models.

A. 2D EMC Model Without Considering Axial Flux Leakage

Fig. 5(a) shows the CMG Geometry in the *XY* plane. Because the CMG can be conveniently expressed in cylindrical coordinates, the permeance elements are expressed in cylindrical

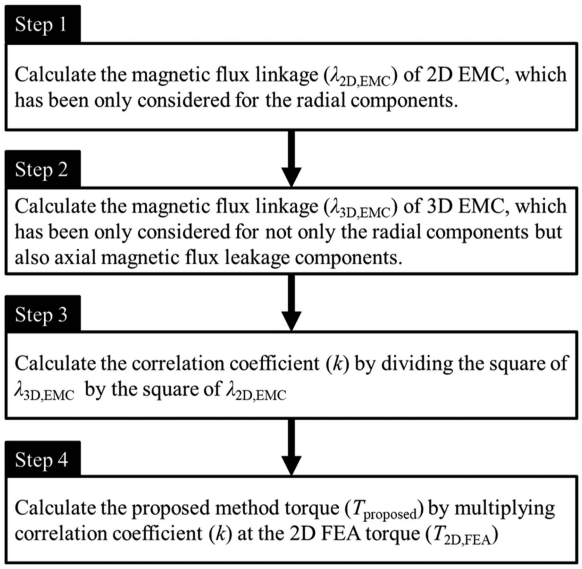

Fig. 4. Proposed method considering the axial flux leakage of CMG through two-dimensional (2D) FEA.

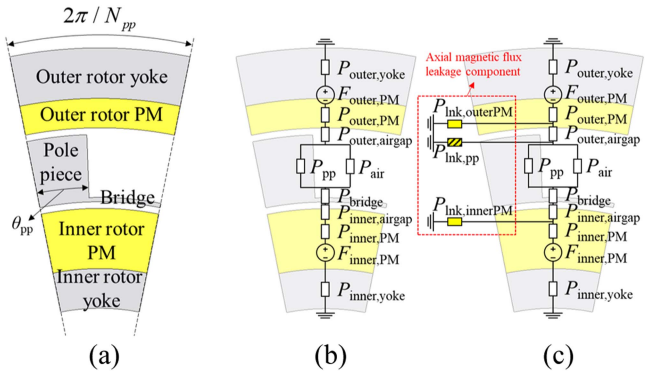

Fig. 5. Equivalent magnetic circuit (EMC) configuration (a) CMG geometry in the *XY* plane. (b) 2D EMC for one PP of the CMG without axial flux leakage. (c) 3D EMC for one PP of the CMG with axial flux leakage.

coordinates. The configuration of the 2D EMC model is illustrated in Fig. 5(b). Therefore, (3) gives $P_{\mathrm{outer,yoke}}$, $P_{\mathrm{outer,PM}}$, $P_{\mathrm{outer,airgap}}$, P_{bridge}, $P_{\mathrm{inner,airgap}}$, $P_{\mathrm{inner,PM}}$, and $P_{\mathrm{inner,yoke}}$, the permeances of the outer rotor yoke, outer rotor PM, outer air gap, bridge, inner air gap, inner rotor PM, and inner rotor yoke, respectively.

$$P_{\mathrm{e}} = \frac{2\pi\mu_{\mathrm{e}} L_{\mathrm{stk}}}{\ln(1 + t_{\mathrm{e}}/r_{\mathrm{e}})}, \tag{3}$$

where μ_{e}, L_{stk}, t_{e}, and r_{e} are the element permeability, stack length of the CMG, thickness of each element, and inner radius of each element, respectively.

Equations (4) and (5) give P_{PP} and P_{air}, the permeance of the PP, and the air between the PP, respectively.

$$P_{\mathrm{PP}} = \frac{\mu_{\mathrm{PP}} L_{\mathrm{stk}} \theta_{\mathrm{PP}}}{\ln(1 + t_{\mathrm{PP}}/r_{\mathrm{PP}})} \times N_{\mathrm{PP}}, \tag{4}$$

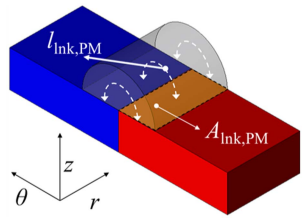

Fig. 6. PM axial flux leakage path.

$$P_{\mathrm{air}} = \frac{\mu_0 L_{\mathrm{stk}} (2\pi/N_{\mathrm{PP}} - \theta_{\mathrm{PP}})}{\ln(1 + t_{\mathrm{PP}}/r_{\mathrm{PP}})} \times N_{\mathrm{PP}}, \tag{5}$$

where μ_{PP}, θ_{PP}, t_{PP}, r_{PP}, and μ_0 are the permeability of the PP, angle of one PP, thickness of the PP, inner radius of the PP, and vacuum permeability, respectively.

Equation (6) gives $F_{\mathrm{outer,PM}}$ and $F_{\mathrm{inner,PM}}$, the MMF of the outer and inner rotors PM, respectively.

$$F_{\mathrm{PM}} = \frac{B_r t_{\mathrm{PM}}}{\mu_0 \mu_{\mathrm{rec}}}, \tag{6}$$

where B_r, t_{PM}, and μ_{rec} are the residual magnetic flux density, PM thickness, and recoil permeability, respectively.

B. 3D EMC Model With Considering Axial Flux Leakage

The configuration of the 3D EMC model is illustrated in Fig. 5(c). The difference between the 2D and 3D EMC is that the axial flux leakages of the PM and PP were considered. Fig. 6 shows the axial flux leakage path and volume at the PM. The axial flux leakage permeance is the mean cross-sectional area divided by the mean flux-path length. The mean cross-sectional area was obtained by dividing the flux path volume by the mean length of the flux path. Eq. (7) gives $P_{\mathrm{lnk,PM}}$ as the flux leakage permeance of the outer and inner rotor PM.

$$P_{\mathrm{lnk,PM}} = \frac{A_{\mathrm{lnk,PM}} \mu_0}{l_{\mathrm{lnk,PM}}} \times 2P_n, \tag{7}$$

where $A_{\mathrm{lnk,PM}}$, $l_{\mathrm{lnk,PM}}$, and P_n are the mean cross-sectional area, mean axial flux leakage path length, and number of PM pole pairs, respectively.

Fig. 7 shows the axial flux leakage path and volume at the PP. The PP has four axial flux leakage permeance elements comprising a semicircular cylinder (SC), half annulus (HA), spherical quadrants (SQ), and quadrants of the spherical shell (QSS) path. Eqs. (8)–(11) provide the axial flux leakage permeance for each element [22].

$$P_{\mathrm{SC}} = \frac{0.322\mu_0 l}{1.22g} = 0.264\mu_0 l, \tag{8}$$

$$P_{\mathrm{HA}} = \frac{2\mu_0 t l}{\pi(g + t)}, \tag{9}$$

$$P_{\mathrm{SQ}} = 2 \times \frac{0.1g^2\mu_0}{1.3g} = 0.154\mu_0 g, \tag{10}$$

$$P_{\mathrm{QSS}} = 2 \times \frac{\pi\mu_0 t(t + g)/8}{\pi(t + g)/2} = \frac{\mu_0 t}{2}, \tag{11}$$

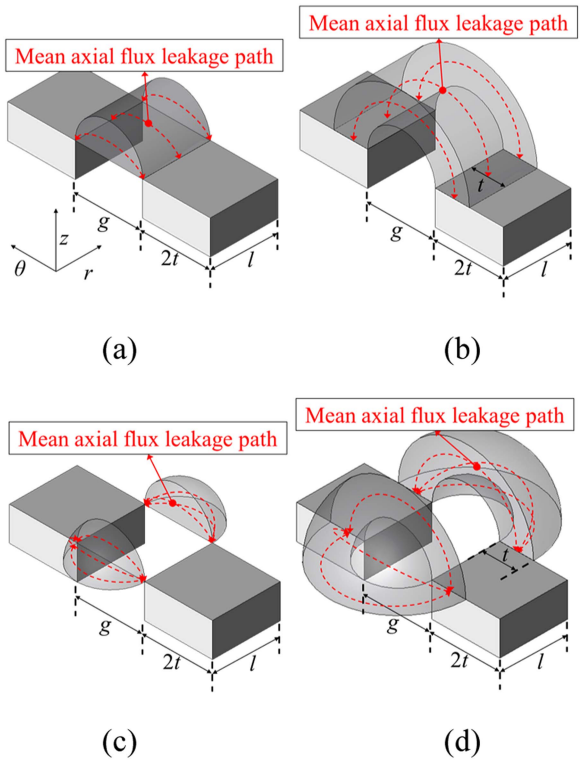

Fig. 7. PP axial flux leakage path. (a) SC path. (b) HA path. (c) SQ path. (d) QSS path.

TABLE II
CMG BASE MODEL DESIGN DIMENSIONS FOR PROPOSED METHOD VALIDATION

Parameter	Value	Unit
Outer / Inner rotor yoke thickness	6	mm
Outer / Inner pole pair	14 / 2	-
Outer / Inner rotor PM thickness	6	mm
Pole piece thickness	5.4	mm
Pole piece bridge thickness	0.5	mm
Pole piece angle	11.25	°
Outer / Inner airgap	0.8	mm
Stack length	30	mm

where l, g, and t are the depth of the flux leakage path, air gap length between the PP, and half-width of the PP, respectively. Therefore, the total flux leakage permeance was calculated as follows:

$$P_{\mathrm{lnk,PP}} = 2 \times (P_{\mathrm{SC}} + P_{\mathrm{HA}} + P_{\mathrm{SQ}} + P_{\mathrm{QSS}}) \times N_{\mathrm{PP}}. \quad (12)$$

C. Correlation Coefficient

Table II lists the design dimensions of the CMG base model used to comparison for 2D EMC, 3D EMC, 2D FEA, and 3D FEA. The magnetic flux change ratio between 2D and 3D EMC of a CMG base model is calculated as follows:

$$\lambda_{ratio} = \left| \frac{\lambda^2_{\mathrm{3D,EMC}} - \lambda^2_{\mathrm{2D,EMC}}}{\lambda^2_{\mathrm{3D,EMC}}} \right| \times 100, \quad (13)$$

where $\lambda_{\mathrm{3D,EMC}}$ is the magnetic flux calculated by the 3D EMC, and $\lambda_{\mathrm{2D,EMC}}$ is the magnetic flux calculated by the 2D EMC.

The torque change ratio between 2D and 3D FEA of a CMG base model is calculated as follows:

$$T_{ratio} = \left| \frac{T_{\mathrm{3D,FEA}} - T_{\mathrm{2D,FEA}}}{T_{\mathrm{3D,FEA}}} \right| \times 100, \quad (14)$$

where $T_{\mathrm{3D,FEA}}$ is the 3D FEA torque, and $T_{\mathrm{2D,FEA}}$ is the 2D FEA torque. The torque change ratio for a CMG base model was 14.97%, and the magnetic flux change ratio was 16.54%, indicating a difference of 1.57 percent points in the change ratio.

Therefore, using the relationships in (13) and (14) for the CMG base model and the fact that torque is proportional to the square of the magnetic flux density in the air gap, the relationship between torque and magnetic flux in the air gap can be expressed as follows:

$$\lambda^2_{\mathrm{3D,EMC}} : \lambda^2_{\mathrm{2D,EMC}} = T_{\mathrm{proposed}} : T_{\mathrm{2D,FEA}}, \quad (15)$$

where T_{proposed} is the torque result calculated by the proposed method.

Then, (15) can be written as follows:

$$T_{\mathrm{proposed}} = \frac{\lambda^2_{\mathrm{3D,EMC}}}{\lambda^2_{\mathrm{2D,EMC}}} \cdot T_{\mathrm{2D,FEA}} = k \cdot T_{\mathrm{2D,FEA}}, \quad (16)$$

where k is the correlation coefficient.

TABLE III
COMPARISON OF TORQUE RESULT AND COMPUTATIONAL TIME OF 2D FEA, PROPOSED METHOD, AND 3D FEA

Method	Torque (Nm)		Computational time (Normalized)	System
	Inner	Outer		
2D FEA	3.73	25.96	1	12th Gen Intel(R) Core(TM) i7-12700K
Proposed method	3.20	22.54	1	
3D FEA	3.19	22.58	288	

The correlation coefficients determined by EMC and the performance of the CMG in 2D FEA can then be used to predict the performance of the CMG in 3D FEA. Table III lists the torque results and computational times for the 2D FEA, proposed method, and 3D FEA of the CMG base model. The FEA models were constructed and calculated using JMAG-Designer software. The torque errors for 2D FEA and 3D FEA, and the proposed method and 3D FEA were 14.79% and 0.18%, respectively. In addition, the computational time for 3D FEA was 288 times greater than that for 2D FEA and the proposed method. For equivalent computation time comparisons, the elements in the radial and tangential directions were the same in the 2D and 3D FEA. The number of elements in 3D FEA increases

TABLE IV
CMG PARAMETER VARIATION RANGE FOR PROPOSED METHOD VALIDATION

Parameter	Range of value	Unit
Outer / Inner rotor yoke thickness	2, 2.2, 2.4, …, 10	mm
Outer / Inner rotor PM thickness		
Pole piece thickness	1.4, 1.6, 1.8, …, 9.4	mm
Pole piece angle	2.25, 2.7, 3.15, …, 20.25	º
Outer / Inner air gap length	0.2, 0.23, 0.26, …, 1.4	mm
Outer pole pair	3, 4, 5, …, 15	-
Inner pole pair	1, 2, 3, …, 13	-
Outer diameter	70, 72, 74, …, 150	mm
Stack length	10, 11, 12, …, 50	mm

proportionally with the stack length; therefore, the longer the stack length, the greater the computational time required by 3D FEA. Therefore, the proposed method can accurately predict the torque in less computational time compared with 3D FEA.

D. Validation of Proposed Method Through Comparison With 3D FEA

To demonstrate the accuracy of the proposed method further, the CMG base model specified in Table II was used as the starting point, and the individual design parameters included in Table IV were independently varied over the range of values specified in Table IV. For example, the outer rotor yoke thickness was varied from 2 to 10, whereas all other parameters specified in Table II were fixed. Fig. 8 shows the 2D FEA, proposed method, and 3D FEA torque variation as the outer/inner rotor yoke thickness variation, outer/inner rotor PM thickness variation, pole piece thickness/angle variation, outer/inner air gap length variation, outer/inner pole pair variation, outer diameter variation, and stack length variation. The length of the air region in the axial direction was set to 6 mm in the 3D FEA to reflect the length of the mean axial flux leakage path, as shown in Fig. 7. For each of these parameters, the proposed method provides very accurate 3D FEA torque predictions for most of the range of values considered; however, there is still an error in the proposed method owing to the linearity assumption and neglect of the elements in the tangential direction. Furthermore, because the radial permeance, as shown in (3), (4), and (5), is dependent on the stack length, and the axial flux leakage permeance, as shown in (8)–(11), is independent of the stack length, applying the proposed method for the same diameter, which is considerably small, may result in similar radial permeance and axial flux leakage permeance values. This leads to an overestimation of the axial flux leakage and an underestimation of the torque when using the proposed method. However, the stack length that satisfies the target specification of 16.8 Nm torque at 110 mm outer diameter set in this article requires a stack length of 23 mm or more based on the CMG base model, and around

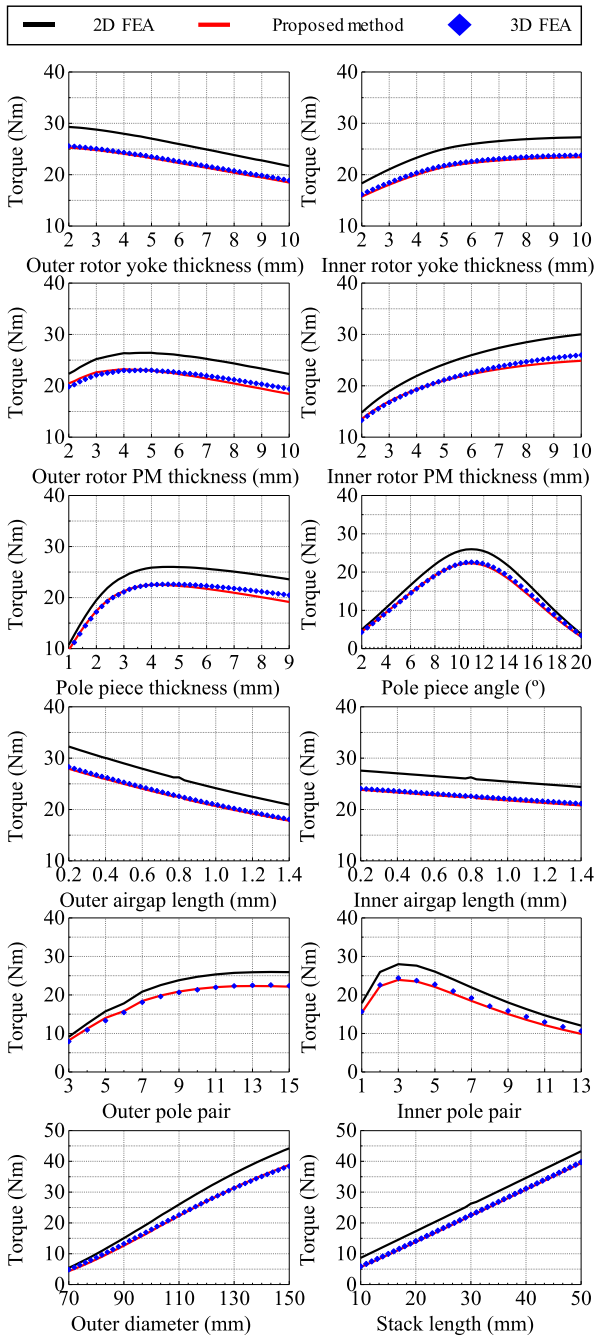

Fig. 8. Variation of the proposed method accuracy with outer/inner rotor yoke thickness, outer/inner rotor pm thickness, pole piece thickness/angle, outer/inner air gap length, outer/inner pole pair, outer diameter, and stack length.

that stack length, the proposed method has a high accuracy in predicting the torque of 3D FEA. The torque of the 2D FEA has an average error of 14.96%, whereas the proposed method has an average error of 2.18%, which shows that the proposed method has a shorter computational time compared to 3D FEA and a higher accuracy compared to 2D FEA.

III. OPTIMUM DESIGN PROCESS

Fig. 9 shows the CMG design process based on the method proposed in Section II. Optimization techniques were applied to

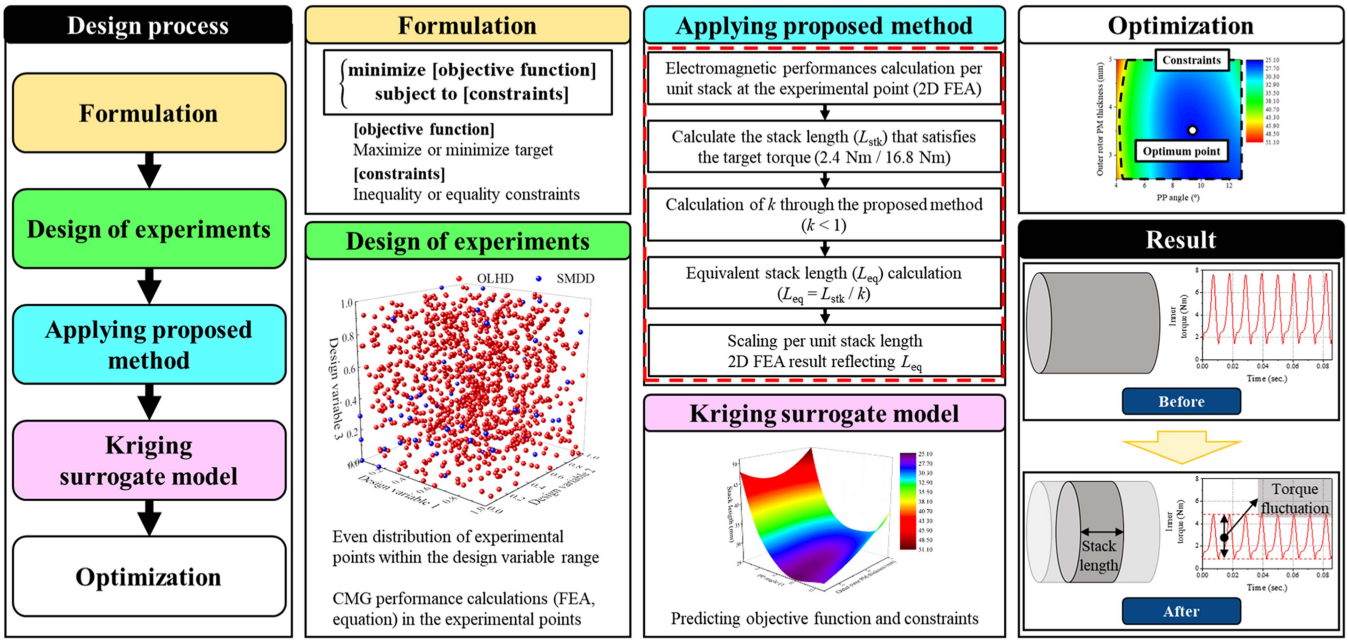

Fig. 9. Proposed CMG design process.

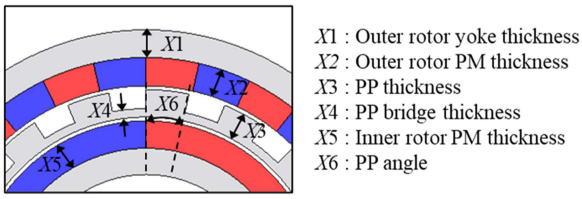

Fig. 10. CMG design variables.

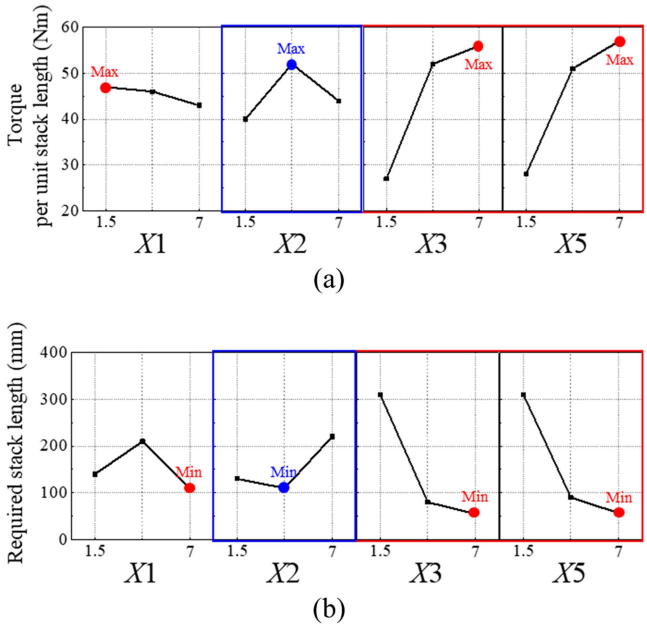

Fig. 11. Main effect plot for (a) torque per unit stack length and (b) required stack length.

the design process. First, an objective function was defined to minimize the stack length of the CMG, peak-to-peak inner rotor torque, and peak-to-peak outer rotor torque. The constraints were set according to the design specifications, such as the torque not being opposite to the direction of rotation and limiting the stack length. Next, the design variables sensitive to the stack length, peak-to-peak inner rotor torque, and peak-to-peak outer rotor torque were determined through sensitivity analysis. Subsequently, a surrogate model was defined by applying the design of experiments (DOE) to the design variables of the selected CMG. Fig. 10 shows the design variables. The design variables determined were the outer-rotor yoke thickness (*X1*), outer-rotor PM thickness (*X2*), PP thickness (*X3*), PP bridge thickness (*X4*), inner-rotor PM thickness (*X5*), and PP angle (*X6*). The thicknesses of the outer/inner rotor PM, outer rotor yoke, and pole piece were determined based on the main-effect plot. Fig. 11 presents the main effect plots of the four design variables. Fig. 11(a), and (b) shows torque per unit stack length and the stack length required to satisfy the target torque, respectively. The thicker the inner rotor PM and pole piece, the higher is the torque per unit stack length, and the required stack length decreases. In addition, the thickness of the outer rotor PM showed nonlinear characteristics; therefore, the range of design variables was determined by considering the geometric dimensions. Fig. 12 shows the required stack length according to the pole piece angle. The angle of one pole of the outer rotor PM was determined as the maximum pole piece angle, and the minimum pole piece angle was determined as the range that did not exceed the design limit of the 45 mm stack length. In addition, the thickness of the bridge was determined to be the maximum considering the minimum thickness of the pole piece, and 0.5 mm was determined to be the minimum considering the

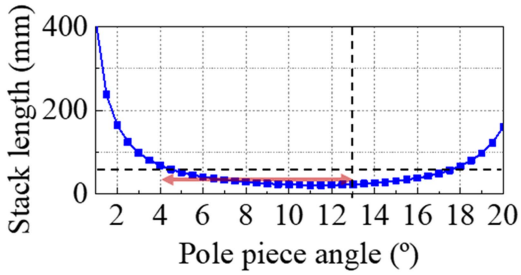

Fig. 12. Required stack length according to pole piece angle.

TABLE V
RANGE OF DESIGN VARIABLES

Parameter	Lower	Upper
$X1$ (mm)	2.5	6
$X2$ (mm)	2.5	5
$X3$ (mm)	3	8
$X4$ (mm)	0.5	1.5
$X5$ (mm)	3	8
$X6$ (°)	4	12.8

fabricability. The ranges of the design variables determined for these reasons are listed in Table V.

As the most important step when applying DOE, a surrogate model is defined by applying the correlation coefficient, which is the proposed method above, according to the design variables. The surrogate model is a functional relationship between the design variable and response, and it ensures low computational time, good accuracy, and very reliable performance. In this article, a kriging surrogate model was applied. Im et al. [23] provided a detailed description of this model. Finally, the kriging surrogate model was used to determine the model that best satisfied the objective function and constraints.

A. Multi-Objective Optimization

Multi-objective optimization involves optimizing more than one objective function under a set of constraints. Multi-objective problems can be solved by combining them into a single-objective scalar function. This method, commonly known as a weighted sum, minimizes the positive weighted convex sum of the objectives. To minimize the stack length, peak-to-peak inner rotor torque, and peak-to-peak outer rotor torque of the CMG, multi-objective optimization was applied. The constraints set the maximum peak-to-peak inner rotor torque to be less than 4.8 Nm, and the maximum peak-to-peak inner rotor torque to be less than 2 Nm, so that torque in the opposite direction does not occur in the direction of rotation. According to design constrains, the stack length was set to be less than the maximum stack length. The formulation of the objective optimization function $f(x_i)$ and its constraints are as follows:

$$\begin{aligned} \text{minimize} \quad & f(x_i) = \alpha_1 L_{\text{stk}} + \alpha_2 T_{\text{PP,in}} + \alpha_3 T_{\text{PP,out}} \\ \text{subject to} \quad & L_{\text{stk}} \le \max(L_{\text{stk}}) \\ & T_{\text{PP,in}} \le \max(T_{\text{PP,in}}) \\ & T_{\text{PP,out}} \le \max(T_{\text{PP,out}}), \end{aligned} \tag{17}$$

where α_1, α_2, and α_3 are the weights, x_i is the design variables, $T_{\text{PP,in}}$ is the peak-to-peak inner rotor torque, $\max(T_{\text{PP,in}})$ is the peak-to-peak inner rotor torque limit, $T_{\text{PP,out}}$ is the peak-to-peak outer rotor torque, $\max(T_{\text{PP,out}})$ is the peak-to-peak outer rotor torque limit, and $\max(L_{\text{stk}})$ is the maximum stack length of CMG. The weight coefficient of stack length α_1 is taken as 0.25, the weight coefficient of the peak-to-peak inner rotor torque α_2 is taken as 0.5, and the weight coefficient of the peak-to-peak outer torque α_3 is taken as 0.25.

B. Design Process Applying the Proposed Method

The part highlighted by the red rectangle in Fig. 9 illustrates the proposed design process. The details of the proposed design method are as follows:

1) The electromagnetic performance per unit stack length at the experimental point set was calculated using DOE.
2) The stack length (L_{stk}) that satisfies the target torque (2.4 Nm / 16.8 Nm) is obtained.
3) The correlation coefficient (k) is calculated using the 2D and 3D EMC.
4) The equivalent stack length (L_{eq}) was calculated by dividing the stack length with the correlation coefficient.
5) The electromagnetic performance of the CMG was determined by scaling the 2D FEA results from 1) to reflect L_{eq}.

The proposed method can be used to predict the electromagnetic performance, such as torque, iron loss, efficiency, and peak-to-peak torque, of a CMG that considers axial flux leakage and satisfies target torque specifications by multiplying the electromagnetic performance of the CMG per unit stack calculated in 1) by the equivalent stack length.

C. Optimum Model

After defining the kriging surrogate model according to the design variables, the optimization algorithm determines the combination of design variables that minimizes the objective function while satisfying the constraints. The optimization algorithm used in this article was SQP. The SQP algorithm offers the advantage of generality, robustness, and efficiency. Furthermore, the second-order information regarding the problem function can be easily integrated. Table VI lists the optimum model that minimizes the stack length of the CMG and the peak-to-peak inner- and outer-rotor torques. To reduce the peak-to-peak inner rotor torque, a two-step skew of 5.625° was applied at the mechanical angle of the inner rotor. Fig. 13 shows the inner and outer rotor torque waveforms of the optimum design model calculated using 3D FEA. When the outer and inner rotor rotation speeds were 50 rpm and 350 rpm, respectively, the inner and outer rotor torques were 2.41 Nm and 16.88 Nm, respectively, and the torque density was 89.55 kNm/m^3. The equation used

TABLE VI
OPTIMIZED DESIGN RESULT OF CMG

Parameter	Value	Unit
Outer rotor yoke thickness	6	mm
Outer rotor PM thickness	3.51	mm
Pole piece thickness	8	mm
Pole piece bridge thickness	0.5	mm
Inner rotor PM thickness	7.17	mm
Pole piece angle	9.23	°
Stack length	24.5	mm
Inner rotor skew angle	5.625	°

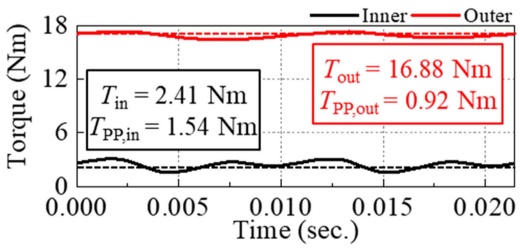

Fig. 13. CMG torque waveforms of the optimal design model calculated using 3D FEA.

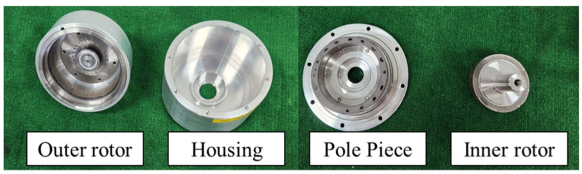

Fig. 14. Fabricated prototype CMG for validation.

to calculate the efficiency of 3D FEA is as follows:

$$\eta_{\mathrm{FEA}} = \frac{T_{\mathrm{FEA,out}}\omega_{\mathrm{FEA,out}}}{T_{\mathrm{FEA,out}}\omega_{\mathrm{FEA,out}} + P_{\mathrm{iron}}} \times 100(\%), \qquad (18)$$

where η_{FEA} is the efficiency in 3D FEA, $T_{\mathrm{FEA,out}}$ is the outer rotor torque in 3D FEA, $\omega_{\mathrm{FEA,out}}$ is the outer rotor speed in 3D FEA, and P_{iron} is the iron loss in 3D FEA. Thus, the efficiency of the optimum model calculated using (18) is 98.39%.

However, the CMG with integer gear ratios still exhibited a high peak-to-peak torque electromagnetic performance. Praslicka et al. explained that using an integer gear ratio for the number of gear pole pair in a CMG result in an increase in the torque ripple, whereas using a non-integer gear ratio can result in a decrease in the torque ripple [24].

IV. EXPERIMENTAL VALIDATION

A prototype of the optimal model was developed to validate the proposed design method. Fig. 14 shows the fabricated CMG prototype used in the tests. Fig. 15 shows the measuring equipment and CMG used for the performance testing. Fig. 16 shows the results of the torque and speed measurements. To

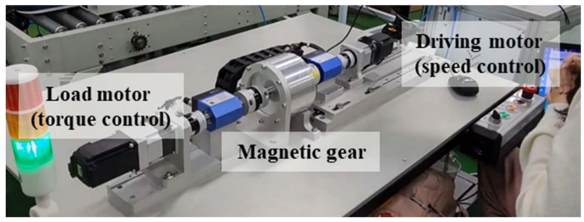

Fig. 15. CMG and test equipment for measuring load performance.

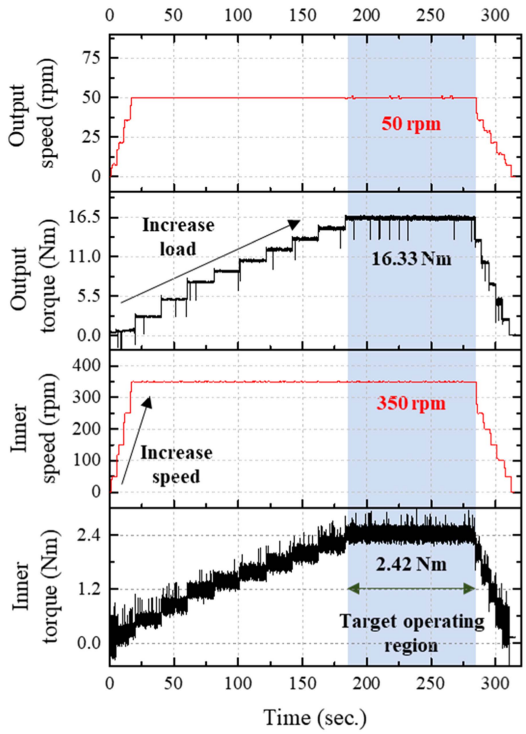

Fig. 16. Experimental validation result for the fabricated prototype CMG.

validate the fabricated CMG prototype, a load experiment was conducted in which an inner rotor rotation speed of 350 rpm and an inner rotor torque of 2.4 Nm were employed to match the target specifications. The inner rotor speed was 350 rpm and the inner rotor torque was 2.41 Nm. The outer rotor speed was 50 rpm, outer rotor torque was 16.33 Nm, and torque density was 86.63 kNm/m^3. The equation used to calculate the experimental efficiency is as follows:

$$\eta_{\mathrm{EXP}} = \frac{T_{\mathrm{out,EXP}}\omega_{\mathrm{out,EXP}}}{T_{\mathrm{in,EXP}}\omega_{\mathrm{in,EXP}}} \times 100(\%), \qquad (19)$$

where η_{EXP} is the experimental efficiency, $T_{\mathrm{out,EXP}}$ and $T_{\mathrm{in,EXP}}$ are the experimental outer and inner rotor torques, respectively, and $\omega_{\mathrm{out,EXP}}$ and $\omega_{\mathrm{in,EXP}}$ are the experimental outer and inner rotor rotation speeds, respectively. Thus, the efficiency of the fabricated CMG prototype, calculated using (19), was 96.21%.

Therefore, the torque ratio of the fabricated CMG prototype was 6.78. Table VII presents the results of the comparative analysis of the 3D FEA and the experimental measurements. The relative error between the experimental torque and the 3D

TABLE VII
COMPARISON OF 3D FEA AND EXPERIMENTAL

Parameter	T_{in} (Nm)	T_{out} (Nm)	Efficiency (%)
3D FEA (without P_{mech})	2.41	16.88	98.39
Experiment (with P_{mech})	2.42	16.33	96.21

FEA torque was less than 3.26%. Furthermore, the difference between the experimental and 3D FEA efficiencies was 2.18%. This efficiency error occurs because the experiment considers mechanical losses, such as bearing and winding losses, whereas 3D FEA does not consider them.

V. CONCLUSION

This article proposed and developed an electromagnetic 3D performance prediction method and design for CMGs. To this end, design optimization was performed on the key parameters of CMGs. The contributions of this article are summarized as follows.

1) The correlation coefficient was calculated through 2D EMC without considering the axial flux leakage path and 3D EMC by considering the axial flux leakage path. The 3D performance prediction method proposed for CMGs was analyzed by combining the performance of correlation coefficients and 2D FEA. The computational times of the proposed method and 3D FEA reveal that the proposed method can reduce the computational time required to predict the CMG performance.
2) The parameters affecting the electromagnetic properties of the CMG were optimized. To reduce the peak-to-peak torque, which is an electromagnetic characteristic of a CMG with an integer gear ratio, multi-objective optimization was performed. The optimum design resulted in a stack length of 24.5 mm and an inner rotor peak-to-peak torque of 1.54 Nm.
3) A CMG prototype was fabricated, and an experimental platform was built to test the electromagnetic characteristics of the CMG, such as the rotational speed and torque of the inner and outer rotors. The results validate the feasibility of the optimum CMG design.

REFERENCES

[1] L. Fang, D. Li, and R. Qu, "Torque improvement of Vernier permanent magnet machine with larger rotor pole pairs than stator teeth number," *IEEE Trans. Ind. Electron.*, vol. 70, no. 12, pp. 12648–12659, Dec. 2023, doi: 10.1109/TIE.2022.3232651.

[2] L. Jing, W. Tang, T. Wang, T. Ben, and R. Qu, "Performance analysis of magnetically geared permanent magnet brushless motor for hybrid electric vehicles," *IEEE Trans. Transp. Electrific.*, vol. 8, no. 2, pp. 2874–2883, Jun. 2022, doi: 10.1109/TTE.2022.3151681.

[3] E. Gouda, S. Mezani, L. Baghli, and A. Rezzoug, "Comparative study between mechanical and magnetic planetary gears," *IEEE Trans. Magn.*, vol. 47, no. 2, pp. 439–450, Feb. 2011, doi: 10.1109/TMAG.2010.2090890.

[4] Y. Wang, M. Filippini, N. Bianchi, and P. Alotto, "A review on magnetic gears: Topologies, computational models, and design aspects," *IEEE Trans. Ind. Appl.*, vol. 55, no. 5, pp. 4557–4566, Sep./Oct. 2019, doi: 10.1109/TIA.2019.2916765.

[5] K. Atallah and D. Howe, "A novel high-performance magnetic gear," *IEEE Trans. Magn.*, vol. 37, no. 4, pp. 2844–2846, Jul. 2001, doi: 10.1109/20.951324.

[6] L. Jian, K. T. Chau, Y. Gong, J. Z. Jiang, C. Yu, and W. Li, "Comparison of coaxial magnetic gears with different topologies," *IEEE Trans. Magn.*, vol. 45, no. 10, pp. 4526–4529, Oct. 2009, doi: 10.1109/TMAG.2009.2021662.

[7] L. Jian and K. T. Chau, "A coaxial magnetic gear with halbach permanent magnet arrays," *IEEE Trans. Energy Convers.*, vol. 25, no. 2, pp. 319–328, Jun. 2010, doi: 10.1109/TEC.2010.2046997.

[8] J. J. Scheidler, V. M. Asnani, and T. F. Tallerico, "NASA's magnetic gearing research for electrified aircraft propulsion," in *Proc. AIAA/IEEE Electric Aircr. Technol. Symp.*, 2018, pp. 1–12.

[9] L. Jing, W. Liu, W. Tang, and R. Qu, "Design and optimization of coaxial magnetic gear with double-layer PMs and spoke structure for tidal power generation," *IEEE/ASME Trans. Mechatron.*, early access, Apr. 11, 2023, doi: 10.1109/TMECH.2023.3261987.

[10] M. Fukuoka, K. Nakamura, and O. Ichinokura, "Dynamic analysis of planetary-type magnetic gear based on reluctance network analysis," *IEEE Trans. Magn.*, vol. 47, no. 10, pp. 2414–2417, Oct. 2011, doi: 10.1109/TMAG.2011.2157100.

[11] M. Johnson, M. C. Gardner, and H. A. Toliyat, "A parameterized linear magnetic equivalent circuit for analysis and design of radial flux magnetic gears—Part I: Implementation," *IEEE Trans. Energy Convers.*, vol. 33, no. 2, pp. 784–791, Jun. 2018, doi: 10.1109/TEC.2017.2777875.

[12] M. Johnson, M. C. Gardner, and H. A. Toliyat, "A parameterized linear 3D magnetic equivalent circuit for analysis and design of radial flux magnetic gears–Part I: Implementation," *IEEE Trans. Energy Convers.*, vol. 36, no. 4, pp. 2894–2902, Dec. 2021, doi: 10.1109/TEC.2021.3061635.

[13] T. Lubin, S. Mezani, and A. Rezzoug, "Analytical computation of the magnetic field distribution in a magnetic gear," *IEEE Trans. Magn.*, vol. 46, no. 7, pp. 2611–2621, Jul. 2010, doi: 10.1109/TMAG.2010.2044187.

[14] H. M. Shin and J. H. Chang, "Analytical magnetic field calculation of coaxial magnetic gear with flux concentrating rotor," *IEEE Trans. Magn.*, vol. 52, no. 7, Jul. 2016, Art. no. 7004404, doi: 10.1109/TMAG.2015.2512587.

[15] H. Zhao, C. Liu, Z. Song, and J. Yu, "A fast optimization scheme of coaxial magnetic gears based on exact analytical model considering magnetic saturation," *IEEE Trans. Ind. Appl.*, vol. 57, no. 1, pp. 437–447, Jan./Feb. 2021, doi: 10.1109/TIA.2020.3040142.

[16] P. O. Rasmussen, T. O. Andersen, F. T. Jorgensen, and O. Nielsen, "Development of a high-performance magnetic gear," *IEEE Trans. Ind. Appl.*, vol. 41, no. 3, pp. 764–770, May/Jun. 2005, doi: 10.1109/TIA.2005.847319.

[17] S. Gerber and R.-J. Wang, "Evaluation of a prototype magnetic gear," in *Proc. IEEE Int. Conf. Ind. Technol.*, 2013, pp. 319–324, doi: 10.1109/ICIT.2013.6505692.

[18] S. Gerber and R.-J. Wang, "Analysis of the end-effects in magnetic gears and magnetically geared machines," in *Proc. IEEE Int. Conf. Elect. Mach.*, 2014, pp. 396–402, doi: 10.1109/ICELMACH.2014.6960211.

[19] S.-H. Lee, S.-Y. Im, J.-Y. Ryu, and M.-S. Lim, "Torque prediction of magnetic gear considering 3D axial leakage flux by equivalent magnetic circuit," in *Proc. IEEE Transp. Electrific. Conf. Expo, Asia-Pacific*, 2022, pp. 1–6, doi: 10.1109/ITECAsia-Pacific56316.2022.9941986.

[20] M. Johnson, M. C. Gardner, and H. A. Toliyat, "A parameterized linear magnetic equivalent circuit for analysis and design of radial flux magnetic gears–Part II: Evaluation," *IEEE Trans. Energy Convers.*, vol. 33, no. 2, pp. 792–800, Jun. 2018, doi: 10.1109/TEC.2017.2777876.

[21] M. Johnson, M. C. Gardner, and H. A. Toliyat, "A parameterized linear 3D magnetic equivalent circuit for analysis and design of radial flux magnetic gears–Part II: Evaluation," *IEEE Trans. Energy Convers.*, vol. 36, no. 4, pp. 2903–2911, Dec. 2021, doi: 10.1109/TEC.2021.3061638.

[22] H. C. Roters, "Calculation of the permeance of flux paths through air between surfaces of high-permeability material," in *Electromagnetic Devices*. Hoboken, NJ, USA: Wiley, 1941, ch. 5, sec. 53, pp. 130–133.

[23] S.-Y. Im, S.-G. Lee, D.-M. Kim, G. Xu, S.-Y. Shin, and M.-S. Lim, "Kriging surrogate model-based design of an ultra-high-speed surface-mounted permanent-magnet synchronous motor considering stator iron loss and rotor eddy current loss," *IEEE Trans. Magn.*, vol. 58, no. 2, Feb. 2022, Art. no. 8101405, doi: 10.1109/TMAG.2021.3080119.

[24] B. Praslicka, M. C. Gardner, M. Johnson, and H. A. Toliyat, "Review and analysis of coaxial magnetic gear pole pair count selection effects," *IEEE J. Emerg. Sel. Topics Power Electron.*, vol. 10, no. 2, pp. 1813–1822, Apr. 2022, doi: 10.1109/JESTPE.2021.3053544.

Seung-Hun Lee received the bachelor's degree in automotive engineering in 2022 from Hanyang University, Seoul, South Korea, where he is currently working toward the Ph.D. degree in automotive engineering. His research interests include design and optimization of electric machines and analysis of electro-magnetic field.

So-Yeon Im received the bachelor's degree in automotive engineering in 2020 from Hanyang University, Seoul, South Korea, where she is currently working toward the Ph.D. degree in automotive engineering. Her research interests include the optimization, design, and system modeling of electric vehicles.

Jun-Yeol Ryu received the bachelor's degree in mechanical engineering and electronic systems engineering from Hanyang University, Ansan-si, South Korea, in 2016, and the Ph.D. degree in automotive engineering with Hanyang University, Seoul, South Korea, in 2023. Since 2023, he has been with Korea Automotive Technology Institute, Cheonan, South Korea, where he is currently a Senior Researcher. His research interests include the design of electric machines and analysis of electro-magnetic field.

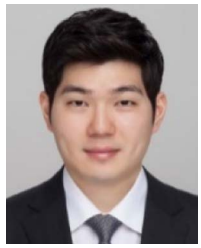

Myung-Seop Lim (Senior Member, IEEE) received the bachelor's degree in mechanical engineering and the master's and Ph.D. degrees in automotive engineering from Hanyang University, Seoul, South Korea, in 2012, 2014, and 2017, respectively. From 2017 to 2018, he was a Research Engineer with Hyundai Mobis, Yongin, South Korea. From 2018 to 2019, he was an Assistant Professor with Yeungnam University, Daegu, South Korea. Since 2019, he has been with Hanyang University, where he is currently an Assistant Professor. His research interests include electromagnetic field analysis and multi-physics analysis of electric machinery for mechatronics systems, such as automotive and robot applications.